Injection Schemes for Improved Flameholding in Supersonic Flow

Corin Segal and Qiuya Tu
University of Florida

Gainesville, Florida, 32611, USA

Previous analyses have shown that mixing can be enhanced using thin pylons that have only a negligible impact on pressure losses. In this study, helium and argon have been transversely injected into a Mach 1.6 airflow simulating a light and a heavy fuel injection behind a thin triangular pylon placed upstream, in the isolator. Penetration and mixing in the test section were observed at three cross-sections including the recirculation region and beyond with planar laser-induced fluorescence (PLIF). Results were compared to the no-pylon cases. The presence of the pylon resulted in improving both penetration and spreading of the jet and, at the same time, in lowering the concentration gradients in the recirculation region, an indication of improved flameholding ability.

Nomenclature

Ar	=	Argon
A_j	=	injector area, mm^2
A_p	=	plume area, mm^2
$C_{acetone}$	=	acetone molar concentration, mol/m^3
$\overline{C}$	=	average of concentration, mol/m^3
C_i	=	instantaneous concentration, mol/m^3
C_i'	=	instantaneous concentration fluctuation, mol/m^3
C_{rms}'	=	standard deviation of concentration fluctuation
f	=	focus length, mm
H	=	step height, mm
He	=	Helium
J	=	jet to crossflow momentum flux ratio
M	=	Mach number
P	=	static pressure, atm
P_{oj}	=	stagnation injection pressure, atm
P_s	=	static pressure at the entrance of isolator, atm
S	=	intensity signal
x	=	streamwise direction
y	=	transverse direction
z	=	spanwise direction

Introduction

The short residence time in practical supersonic combustion systems, typically of the order of a few milliseconds imposes severe requirement for mixing - and vaporization if liquid fuels are used - to ensure efficient heat release and positive net thrust generation[1]. The issue of mixing enhancement is, therefore, of particular interest for these devices.

Various types of fuel injection configurations and injector shapes have been studied for mixing enhancement mostly focused on changing the flowfield within the combustor[2,3]. Straight or swept ramps that produce near parallel injection have shown reasonable far-field mixing[4,5,6], although their near-field mixing performance falls below transverse injection alternatives. The ramp vortex shedding provides a means to lift the fuel from a low injection angle and promotes penetration into the core air stream. Because physical inflow ramps require cooling, especially in localized hot spots such as in recirculation regions, the aerodynamic ramp[7,8] or an angle-injection solution[9,10] from a flush-wall have been suggested as non-cooled injection configurations.

A solution that takes advantage of the high penetration of transverse injectors without the penalty of high pressure losses are the pylon-based injectors suggested by Vinogradov and Prudnikov[11]. It involves thin, swept pylons with the fuel injected transversely in the separated region behind them. The results showed that the penetration increase with these pylons was substantial. Livingston et al[12] showed that thin pylons can be used with minimal pressure losses and applied this type of injection in an inlet, upstream of the isolator to provide additional mixing length. Hence, it is possible to achieve considerable penetration with relatively low dynamic pressure ratios, even less than unity, using this type of pylons. This is significant in particular when considering that in most cases normal injection from the wall requires dynamic pressure ratios of the order of 10-15[13]. A review of thin pylons applications is given by Vinogradov et al[14].

To increase the residence time and achieve a higher degree of mixing in the combustion chamber it may be useful to inject part of the fuel upstream, in the isolator, in the inlet or further upstream on the vehicle body. In this case a complex but more flexible system is obtained; the optimization of this system could result in multiple advantages including (i) mixing enhancement; (ii) shorter isolator and combustor, consequently, reduced weight and cooling loads; (iii) a more flexible fuel control system due to the possibility of distributing the fuel between the preinjection region and the combustor and (iv) the possibility of injecting combinations of liquid and gaseous fuels in different regions[1,15].

When the fuel is injected upstream, there is a danger of flashback due to fuel remaining in the boundary layer potentially causing upstream flame propagation. With the pylons described here penetration increases and the residual fuel in the boundary layer is avoided. Owens et al[15], Shikhman et al[16], Vinogradov et al[17] and Guoskov et al[18] showed in combustion experiments that fuel injection upstream of the combustion chamber was possible without flashback. The same is true for liquid-fuel injection as shown by the experiments by Livingston et al[12] where, in an inlet operating at M = 3.5, the pylon helped to remove the fuel entirely away from the wall. Most significantly, from the mixing enhancement point of view, the jet experienced an abrupt breakup and was carried into the inlet core airflow at the pylon height. Hence, the pylon's presence helped placing the fuel in a favorable mixing region.

More recently, Gruber et al[19] confirmed these results evaluating pylon-aided fuel injection with three pylon geometries. In all cases the presence of the pylon resulted in improved fuel penetration without leading to significant total-pressure-loss characteristics. Computationally, Pohlman and Greendyke[20] obtained similar results using five triangular pylons.

In the study described here, light (Helium) and heavy (Argon) gases were injected transversely through a circular injector in the base of the pylon located in the isolator ten steps (10*H*) upstream of the flameholding region. Several dynamic pressure ratios were applied. The isolator entrance Mach number was 1.6. Penetration, spreading and mixing were measured via acetone PLIF at three axial locations in the test section beginning with the recirculation region. The results were, then, compared with the corresponding no-pylon cases. Considerable improvements in mixing have been observed when the pylons were present.

Experiment Facility and Technique

A. Facility

The facility used here has been described in detail elsewhere[21]. This continuously operating wind-tunnel, shown in Fig. 1 is based on a vitiated heater electronically controlled by a hybrid fuzzy logic controller. The nozzles are interchangeable to provide a range of isolator's entrance Mach numbers from 1.6 to 3.6. All the experiments presented here were conducted at Mach 1.6 and stagnation temperature 300 K. The facility's stagnation pressure was maintained at 4.8 atm.

Both isolator and the test section have quartz glass windows for optical access. The isolator has a constant cross sectional area, 25 × 25 mm^2. The combustion chamber has a rearward facing step with height *H*=12.5 mm acting as a quasi two-dimensional flameholder.

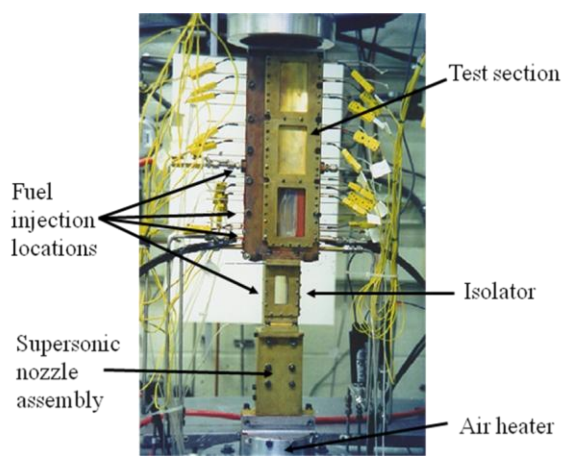

Fig. 1 Supersonic combustion facility.

B. Pylon Injector and Experimental Conditions

Gaseous helium (He) and Argon (Ar) were used as injectants to simulate a light fuel (hydrogen) and a heavy fuel, e.g., propane to evidence the effect of molecular weight. The fuel was transversely injected into the supersonic crossflow from a 1 mm diameter orifice located at 10 upstream of the step, in the isolator as shown in Fig. 2. Two different stagnation injection pressures were applied: 2.4 atm and 5.1 atm. Both pylon and non-pylon configurations were evaluated. The pylon was designed as shown in Fig. 2, to minimize the aerodynamic drag; hence, the thickness was selected as 2.3 times the injector diameter with swept leading edge and triangular cross section based on previous design recommendation[11].

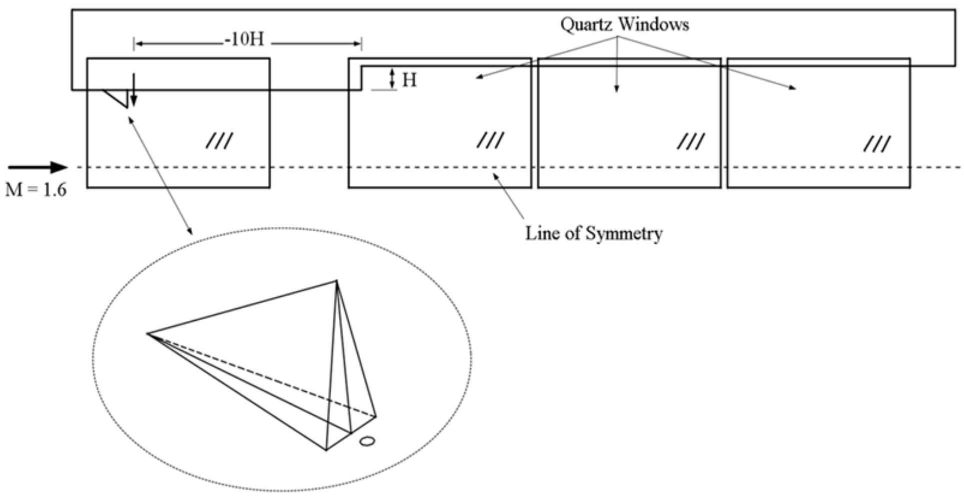

Fig. 2 Isolator and combustion chamber schematic and pylon geometry. The fuel was transversely injected into the supersonic crossflow from a 1mm-diameter orifice located at 10*H* upstream of the step, i.e. in the isolator. The pylon is 7.5 mm high and 2.3 mm wide at the base. Windows allow flow access for PLIF and visualization in the isolator and the test section.

C. Acetone PLIF

Figure 3 illustrates schematically the acetone PLIF system used for measurements. The fourth harmonic from a Spectra-Physics Nd: YAG laser (GCR-150) was used with a wavelength of 266 nm and output energy of 0.75W at 10 Hz. The beam was expanded into a two-dimensional sheet of 50 mm wide and 0.5 mm thick. The optical path included three mirrors, two cylindrical convex lenses of f = 100 mm and 500 mm, and one cylindrical concave lens f = - 100 mm, so that the flowfield could be probed with a vertical laser sheet. The fluorescence images were recorded using an intensified digital charge-coupled device (ICCD) camera with a 1024 ×1280 array and a Sigma 50-mm f/2.8 camera lens. The camera gate was set to 10 ns to collect the acetone fluorescence's life time of 4 ns. The devices were synchronized by a pulse generator. A band pass filter (335-610 nm) and a short pass filter (~500 nm) were placed in front of the camera to eliminate elastic light reflections. The spatial resolution of the camera was 62.5, 104.2, and 63.3 μm/pixel for plane 1, 2, and 3, respectively. The injectant density change due to acetone seeding was estimated to be less than 1.4% assuming saturated condition at the injector. Therefore, this level of acetone seeding caused a negligible influence on the injectant density.

The intensity of laser-induced fluorescence from the acetone molecule depends on the local temperature, pressure, mole-fraction, and the coexisting species and the intensity of the signal S was translated into the acetone molar concentration $C_{acetone}$ (mol/m^3) [22]. The error was estimated to be 6.5% when assuming a linear relationship by the method described in Ref. 23. Figure 4 shows the step and the location of three laser sheet planes. The injection was at 10H upstream of the step and the laser sheet planes were at 0.5H, 2H and 10H downstream of the step, hence in the recirculation region close to the step, towards the end of the recirculation region - since the reattachment was at 2.7H – and further downstream in the far field.

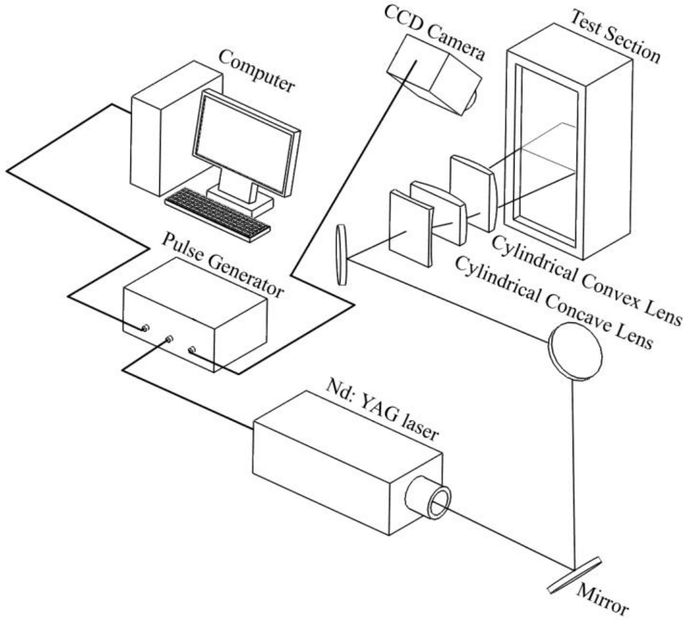

Fig. 3 Schematic of acetone PLIF measurement system. The laser beam was expanded into a two-dimensional sheet of 50 mm wide and 0.5 mm thick at three heights along the vertically oriented test section.

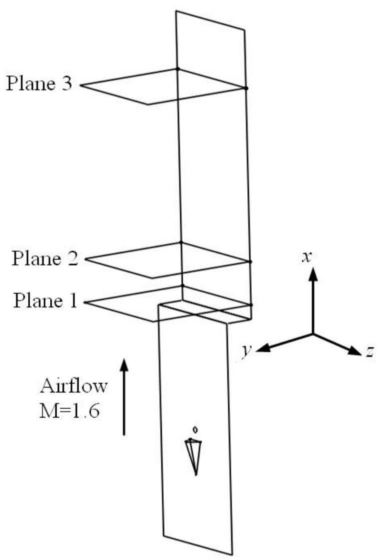

Fig. 4 Location of the selected flow planes. The injection was at 10*H* upstream of the step and the laser sheet planes were at 0.5*H*, 2*H* and 10*H* downstream of the step. The *x*, *y*, *z* axis correspond to the streamwise, transverse and spanwise direction. The three planes investigated are in the recirculation region close the step, towards the end of the recirculation region – since the reattachment was at 2.7*H* downstream from the step – and further downstream in the far field.

Results and Discussions

A. Schlieren Photograph and Pressure Distributions

Figure 5 is a schlieren photograph of the air flow before fuel injection showing the isolator and the combustion chamber. There are weak Mach waves in the isolator due to a slight misalignment of the nozzle and isolator interface. In the combustor the air flow expands around the step and reattaches at 2.7*H*[24]. The recirculation region formed behind the step receives different amounts of fuel depending on presence of the fuel injection in the isolator in this case, or downstream as done in other configurations. The resulting composition has a critical effect in the flameholding ability[25].

The test section wall pressure distribution shown in Fig. 6, (a) for He and (b) for Ar indicates that there is a pressure increase of 0.2 atm immediately behind the pylon and no difference downstream the step. It should be noted that the isolator pressure rise is local, behind and aligned axially with the pylon without effect in the rest of the flow[15] indicating that the presence of the pylon causes essentially no pressure loss.

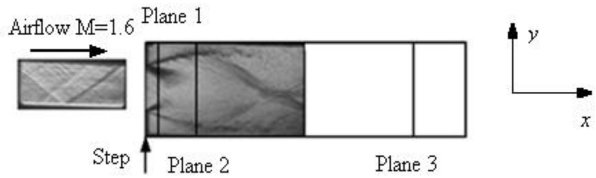

Fig. 5 Schlieren photograph of the air flow without injection or pylon[24]. The black lines indicate the positions of the laser sheet for subsequent PLIF.

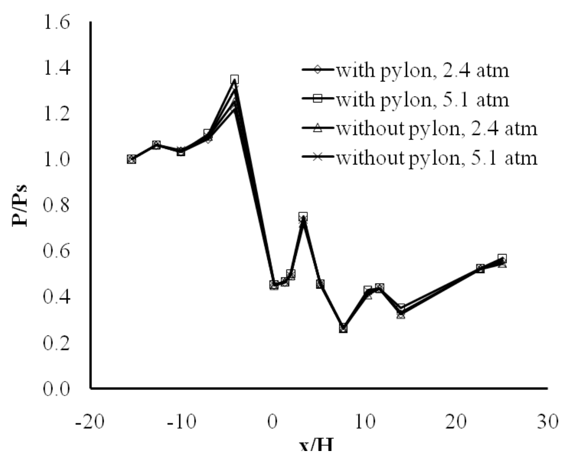

a) Ar

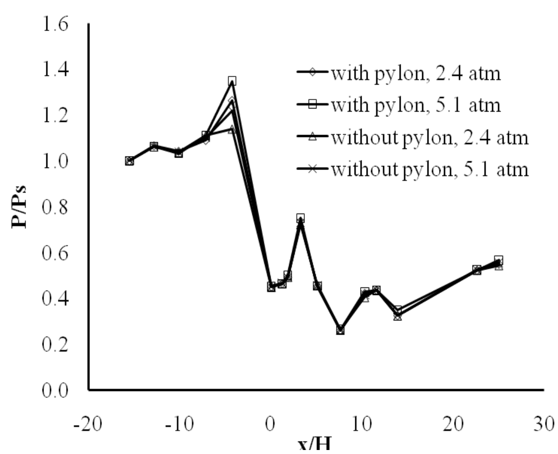

b) Ar

Fig. 6 Normalized pressure distribution at different stagnation injection pressures. There is a slight pressure increase of 0.2 atm behind the pylon and no difference downstream the step in the combustion chamber. This indicates that the pylons cause no significant loss**.**

B. PLIF Results

Instantaneous and ensemble-averaged images described below provide details of the flow structure emphasizing the details of penetration and spreading, two main factors influencing fuel-air mixing.

Instantaneous Structures

Figure 7 presents representative instantaneous PLIF images taken at the selected 3 planes for four cases, which correspond to *x/H* = 0.5, 2, and 10 downstream of the step, hence, the first two planes are in the recirculation region and the third is further downstream. In each image, the main flow direction is out of the paper plane, the axes are normalized by the step height, *H*. The origin is placed at the center of the duct in the *y* direction and at the step in the axial direction, *x*. The injection location is in the isolator at *z/H* = 0, *x/H*= -10 and *y/H* = -1. The LIF intensities are normalized by the maximum intensity in each plane. The highlighted white solid line shows the step. Due to symmetry only half of the duct is shown in fig. 7.

The instantaneous images show to a certain extent the turbulent structures which include both the vortical structures and the flow turbulence effects. In the near-field a compressibility effect is noticed due to molecular weight differences creating a difference in the structure size. But in the far-field the compressibility effect seems to weaken because almost no difference in structure sizes is noticed.

Without the pylon the fuel penetrates rapidly in the recirculation region through the shear layer but remains confined to a small region. With the pylon the instantaneous structure is larger and it stretches in vertical direction while in non-pylon cases the plume occupies a smaller region indicating less penetration and spreading. The structure due to the shear [26, 27] effect is seen at the periphery of the jet plume. In some cases part of the plume is removed from the rest as seen in plane 3 as shown in Fig. 7c. Moreover, the jet plume often reaches the opposite wall for pylon-assisted cases. For the higher molecular weight injectant, i.e., argon, most of the injectant remains close to the injection wall, an effect of lower diffusion.

The instantaneous image results reveal the complex nature of the injectant/air interaction, which is principally responsible for mixing; they also indicate that highly intermittent and dynamic features still exist in the far-field. The main effect of the pylon is to create the low-pressure region behind it leading to increased penetration, however, as a secondary effect, weak vortical structures induced by the pylon help enhance spreading and mixing.

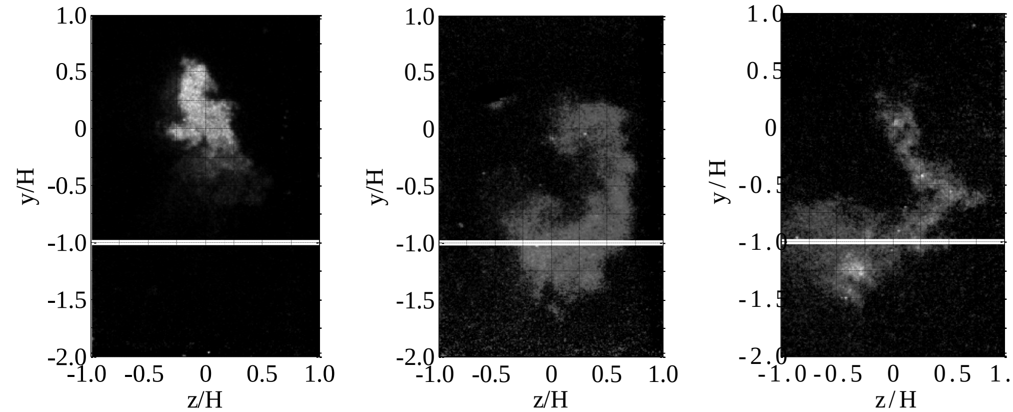

(a) He-injection with -pylon

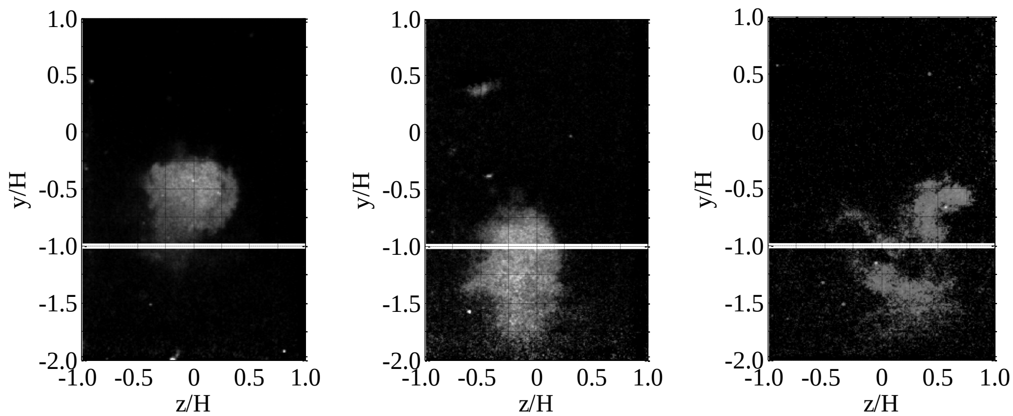

(b) He-injection without -pylon

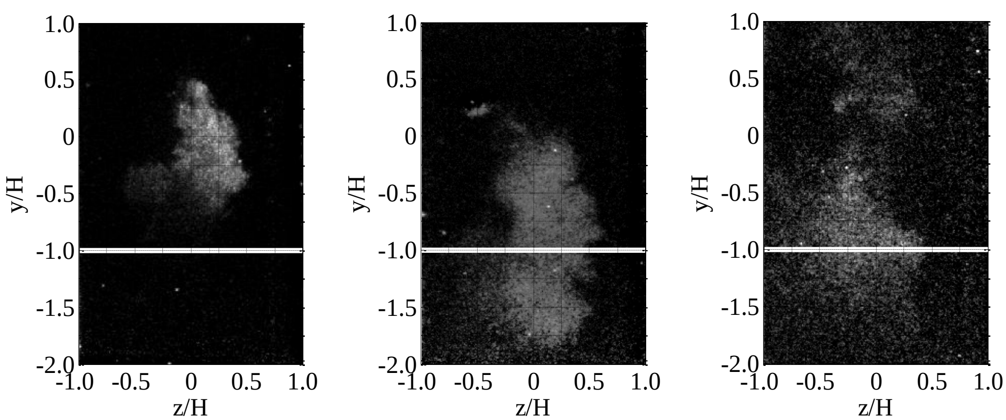

(c) Ar-injection with -pylon

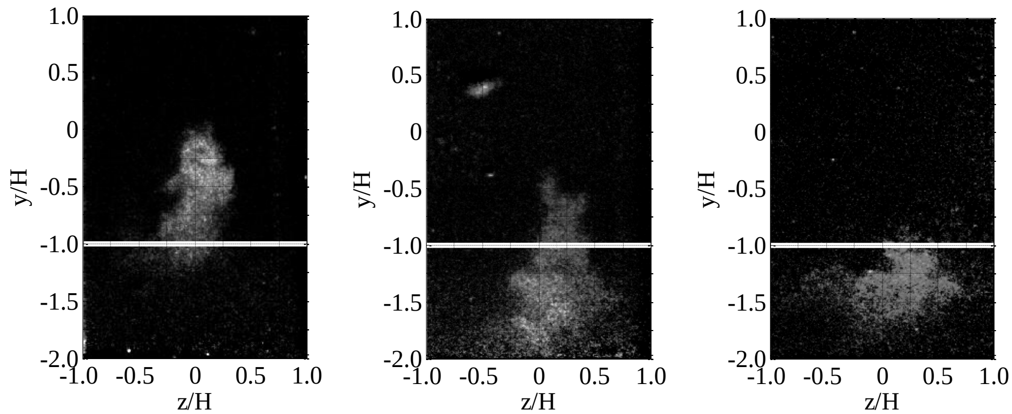

(d) Ar-injection without -pylon

Fig. 7 Instantaneous end-view PLIF images in three measurement planes for four different injection cases: plane 1 (left), plane 2 (center), and plane 3 (right). Air flow direction is out of the paper plane, and the injection location is z/H = 0 and x/H = -10, white solid line at y/H = -1 represents the step height.

Ensemble-Averaged Structures

Figure 8 through 11 show ensemble-averaged PLIF images for each injectant and injection pressure, with plane 1, plane 2, and plane 3 shown from left to right. For each image 300 single shot frames were used for averaging plane 1 and 2 and 600 frames were used for plane 3 since the latter showed weak intensities. The effects of injection pressure and molecular weight are described below.

Effect of Injection Pressure

Figure 8 shows the He injection with the pylon. At lower injection pressure, seen in Fig. 8a, for each plane the core of the plume is closer to the injection wall and the penetration is shorter than those in Fig. 8b, where the pressure was higher. In planes 2 to 3 the spreading dominates with little increase of penetration as the injection pressure is increased. In plane 1 the core of the jet approaches the chamber centerline, at y/H=0, in plane 2 the core of the triangularly shaped plume with wider spread is pushed toward the wall by the airflow expansion around the step and increases again after the reattachment point as shown in plane 3, a characteristic shape with top central part penetrating far into the core flow and even wider spread, almost reaching the side walls. The plume development for Ar injected behind the pylon, seen in Fig. 9, shows a similar trend as He: higher injection pressure enhances penetration with the plume shape changed from triangular in plane 2 to the widely spread shape in plane 3.

Without the pylon, at higher injection pressure He injection, Figure 10 shows an elongated shape in plane 1 and becomes almost round further downstream. It is lifted from the injection wall with some increase of penetration to the step height and spreading, while at lower injection pressure a triangular shaped plume appears in plane 1 and at the end of recirculation region. Further downstream it remains close to the injection wall but it spreads more reaching the side walls. Figure 11 shows the plume images of Ar without pylon, with a similar development as He; at higher injection pressure the spreading is narrower but penetration is higher.

Penetration scales with the fuel-to-air momentum flux ratio[28], J, hence higher injection pressure increases the penetration regardless of the presence of pylon. Although previous studies have shown that the presence of pylons reduces spreading[19], here both penetration and spreading are increased and, furthermore, penetration is increased at higher injection pressure. The additional effect on spreading is due, likely, to the presence of 3-D flow structure following expansion around the 2-D step as a result of the vortical motion induced by the presence of side walls.

Effect of Molecular Weight

When the pylon is present the jet plume axial development is similar for He and Ar with several notable differences. In plane 1 close to the step Ar penetrates less than He whereas in the far-field, at plane 3, the penetration is much higher at lower injection pressure as shown in Figures 8 and 9. Without the pylon there is no penetration difference between the two injectants as shown in Figures 10 and 11 but Ar has a wider spreading and a larger plume area than He in every corresponding case. Thus, it appears that the molecular weight has only a small effect on the plume penetration in agreement with the observations of Portz and Segal[29] and Burger et al[30], although the heavier injectant can enhance spreading even without the aid of the pylon

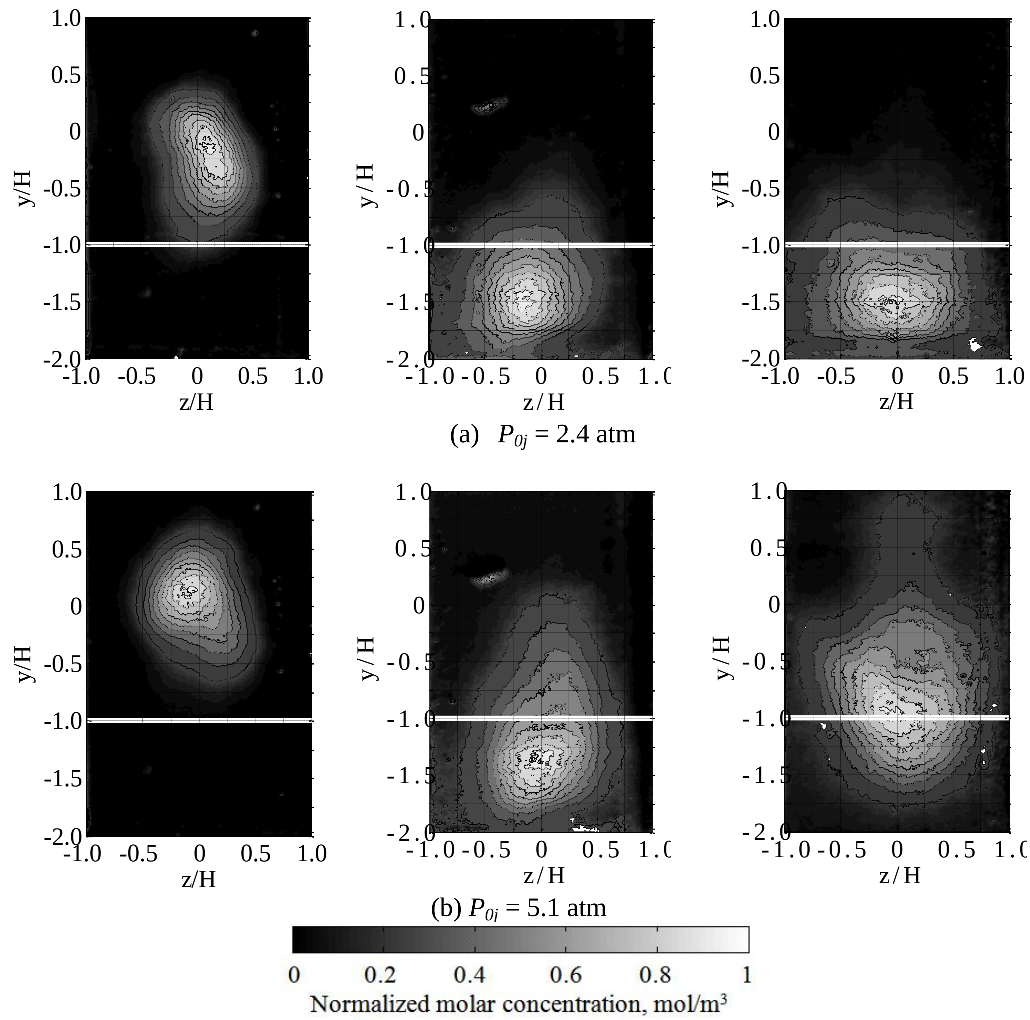

Fig. 8 Averaged end-view PLIF images for He-injection with-pylon cases at two different injection pressure: (a) P_{0j}=2.4 atm, and (b) P_{0j}=5.1 atm. Images in planes 1, 2 and 3 are shown from left to right, air flow direction is out of the paper plane, and the injection location is z/H = 0 and x/H = -10. The solid line at y/H = -1 represents where the step height is.

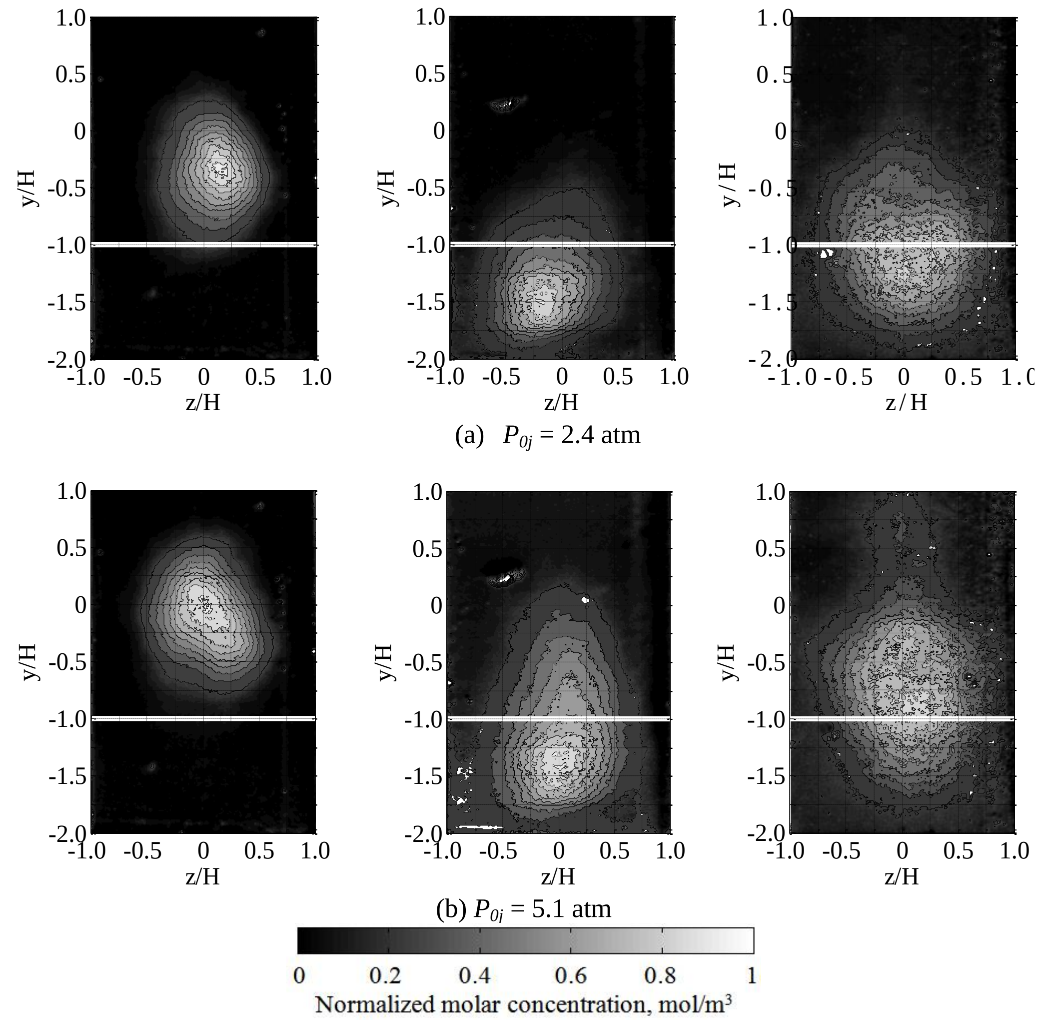

Fig. 9 Averaged end-view PLIF images for Ar-injection with-pylon cases at two different injection pressure: (a) P_{0j}=2.4 atm, and (b) P_{0j}=5.1 atm.

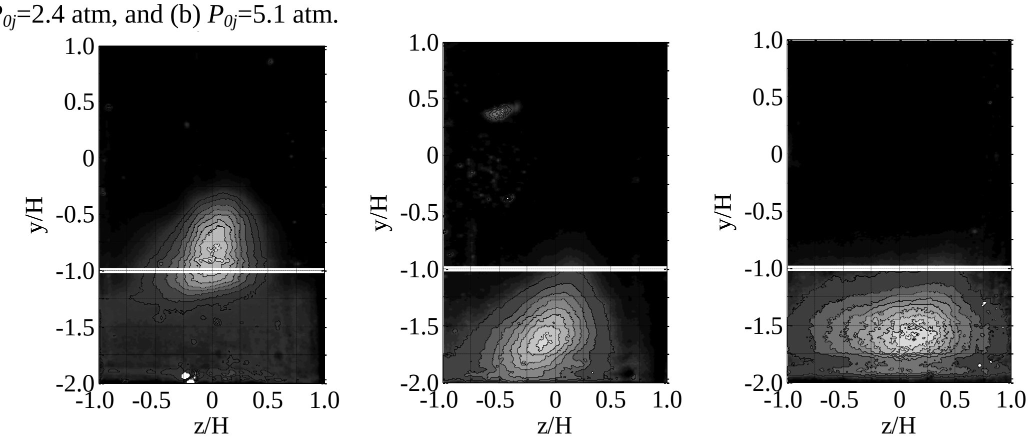

(a) P_{0j} = 2.4 atm

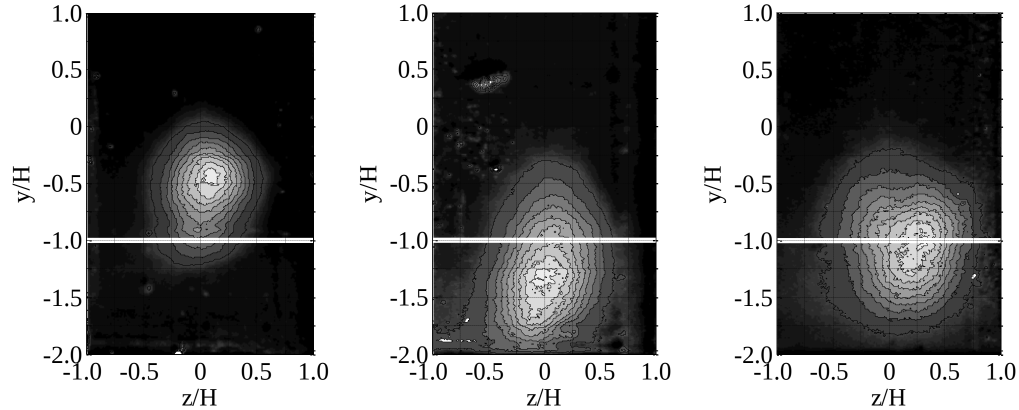

(b) P_{0i} = 5.1 atm

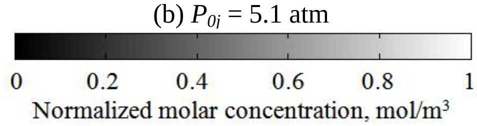

Fig. 10 Averaged end-view PLIF images for He-injection without-pylon cases at two different injection pressure: (a) P_{0j}=2.4 atm, and (b) P_{0j}=5.1 atm.

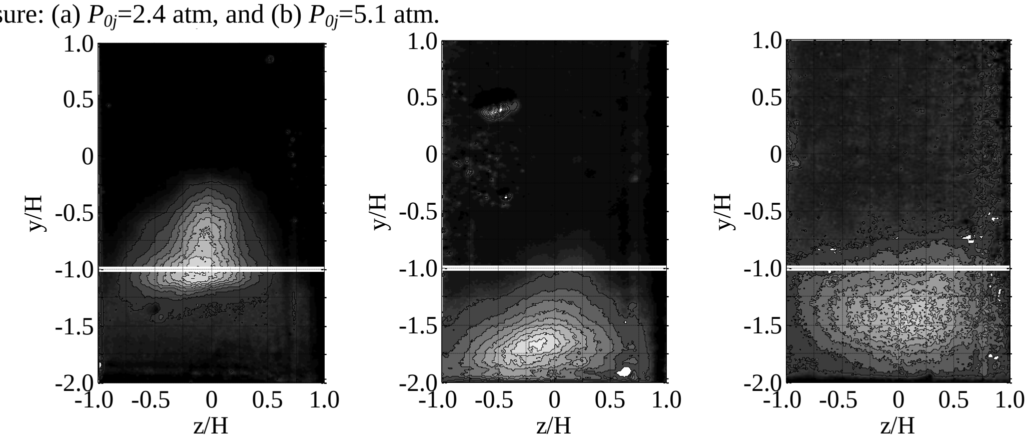

(a) P_{0j} = 35 psi

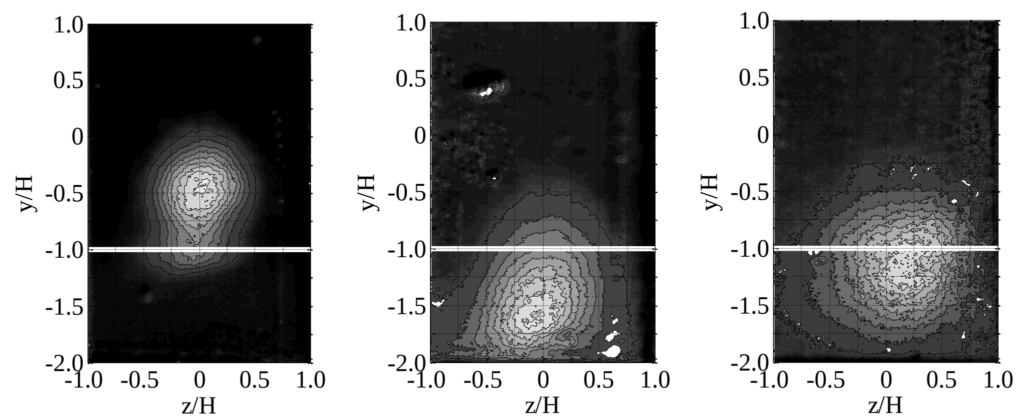

(b) P_{0i} = 75 psi

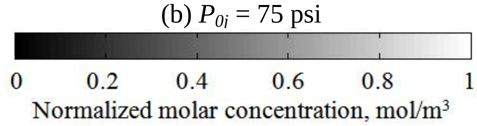

Fig. 11 Averaged end-view PLIF images for Ar-injection without-pylon cases at two different injection pressure: (a) P_{0j}=2.4 atm, and (b) P_{0j}=5.1 atm.

Geometrical Features of Jet Plume

Figures 12 to 14 show certain salient features of the ensemble-averaged images including the plume area, penetration and lateral spreading. The 10% contour of the maximum intensity was taken as the jet plume boundary. The plume penetration *y* was determined from the peak location of this contour, and the lateral spread *Δz* was determined from the widest extend of it; both were normalized by the step height. To avoid any noise in the data, the pixels inside the 30% contour were counted as the plume area normalized by the injector area.

For every case the plume area gradually became larger except for He from plane 2 to plane 3 at 2.4 atm with pylon and at 5.1 atm without pylon as shown in Fig. 12. At higher injection pressure the plume area increased regardless of the pylon's presence but with the pylon the increase was larger. The increase is most significant at higher injection pressure with pylon from plane 1 to plane 2. Figure 13 shows the plume penetration. For Ar the penetration was higher at higher injection pressure and the presence of pylon enhanced it. For He, except in the case with pylon, at higher injection pressure the penetration showed the same trend as Ar, while in other cases the penetration decreased from plane 2 to plane 3. This is due to the presence of the side walls at plane 3 that limit the plume spreading in the far-field. For both injectants, with the pylon present the spreading was narrower than without the pylon.

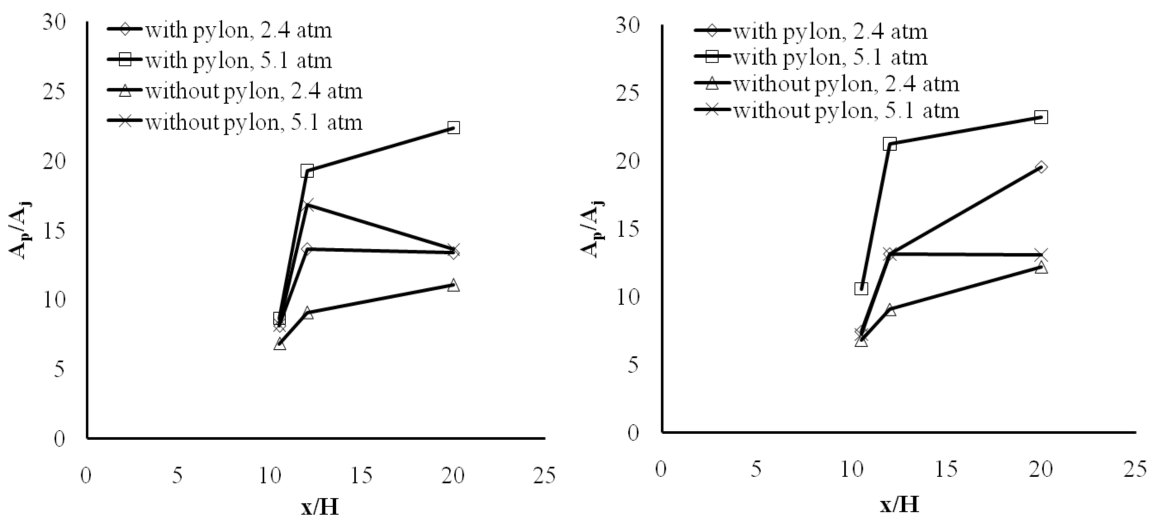

(a) He (b) Ar

Fig. 12 Plume area comparison for each four cases along the streamwise direction for He (a) and Ar (b). In order to obtain the area, the pixels within the contour of 30% value of the maximum intensity in each ensemble-averaged image were counted

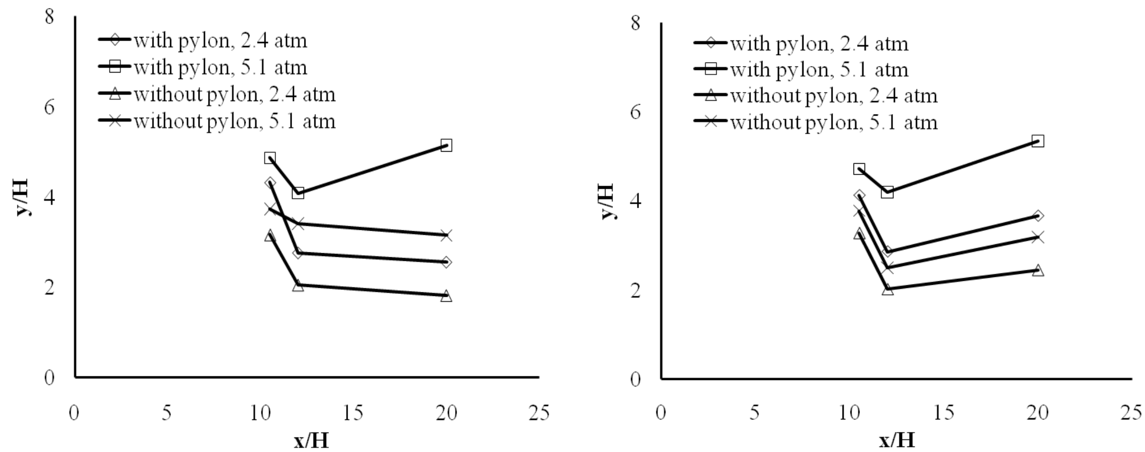

(a) He (b) Ar

Fig. 13 Plume penetration comparison for each case along the streamwise direction for He (a) and Ar (b). The plume penetration was determined by the peak location of the 10% contour of the jet plume.

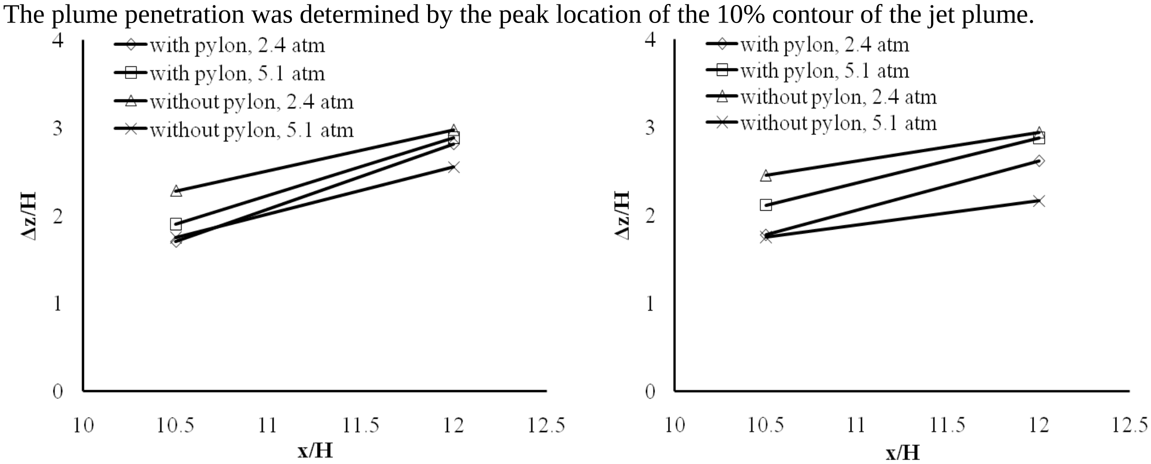

(a) He (b) Ar

Fig. 14 Plume spreading comparison for each four cases along the streamwise direction for He (a) and Ar (b). The lateral spread $\triangle z/H$ was determined from the widest extend of the 10% contour of the jet plume.

Statistical Analysis

Since the fluorescence signal represents the jet molar concentration, the spatial correlation of the PLIF signal fluctuations expresses the spatial extent of the turbulent scalar field. The single-time two-point spatial correlation analysis is useful to clarify the behavior of the turbulent structure[27, 32, 33]. The correlation coefficient $r(\triangle y, \triangle z)$ based on the concentration fluctuation is computed from Eq. (1)

$$\overline{C}(y,z)=\frac{1}{N}\sum_{i=1}^{N}C_i(y,z),\quad C_i'(y,z)=C_i(y,z)-\overline{C}(y,z),\quad C_{rms}'(y,z)=\sqrt{\frac{1}{N}\sum_{i=1}^{N}C_i'^2(y,z)},\qquad i=1,2,\cdots,N$$
$$r(\Delta y,\Delta z)=\frac{\frac{1}{N}\sum_{i=1}^{N}\left[C_i'(y,z)\cdot C_i'(y+\Delta y,z+\Delta z)\right]}{C_{rms}'(y,z)\cdot C_{rms}'(y+\Delta y,z+\Delta z)} \tag{1}$$

where point (y, z) is the reference used for features correlation[31], $C_i(y,z)$ is the instantaneous concentration, $C_i'(y,z)$ is its fluctuation, $\overline{C}(y,z)$ is the average of concentration, $C'_{rms}(y,z)$ is the standard deviation of concentration fluctuation, Δy and Δz are the spatial differences in y and z directions, respectively. In the present study, the significantly correlated region with a sample size N of 300 was chosen where the absolute value of the correlation coefficient $|r| \geq 0.16$, as determined by statistical testing. In Figure 15 each correlation map is depicted with the contour levels varying in increments of 0.1 in $0.2 \leq |r| \leq 1.0$. Also, the line of r = 0.16, which indicates the boundary of the highly-significantly correlated regions, are highlighted with black solid line. The contours of 0.1 and 0.5 in averaged plume intensities are plotted as well, for reference. The reference points for calculating the correlation maps are the bottom edge of the 0.5 contour since the concentration fluctuation is the most intensive on the 50% contour[32]. For correlation analysis of this end-view image, 300 single-shot images were used. The computed domain was 340 pixels high by 510 pixels wide for plane 1 and 432 pixels high by 648 pixels wide for plane 3, corresponding to $-2.0 \leq y/H \leq 1.0$, $-1.0 \leq z/H \leq 1.0$. The spacing used for this correlation covered five pixels, corresponding to 0.029H or 0.0046D for plane 1 and 0.023H or 0.0036D for plane 3. This spacing is small enough to resolve the turbulent structure[32].

Figure 15 shows correlation maps for He-injection cases in plane 1. Clearly, the highly correlated region is seen around the reference point. The high correlation region is found around the reference point. For all cases, the negative correlation region, shown in Figure 15 with grey shades, appears symmetrically to the correlated region, shown with white shades, around the plume center. This indicates that the fluid in the negative region decreases while the fluid around the reference point increases in the given cross-section. Since the averaged plume shape suggests the entrainment of the fluid into the step base, this behavior indicates that the fluid in the upper part of the plume displayed as the negative correlation enters into the step base region.

In general in the pylon cases the highly-correlated region is compact and well-organized regardless of the injection pressure. Without the pylon the correlated region is not well organized and expands to the lower region of the duct. These results indicate that there exists a relatively large-scale turbulent structure in this plane and an expectation of enhanced mixing in the step base.

At plane 3 Figure 16 shows a different trend. In every case the highly correlated region is small. The negatively correlated region that implies the entrainment of fluid in a downward direction is no longer seen, similarly to the results in ref. 32. The region where the large-scale structure is absent has a small correlation region. Therefore in the lower-pressure case both with and without the pylon there seems no exit no large-scale structure. In the higher-pressure cases a correlation region appears but it is considerably smaller than the one at plane 1.

These observations indicate that at plane 1 the flow is dominated by relatively large-scale turbulent stirring and at plane 3 shear-induced structures are prevalent.

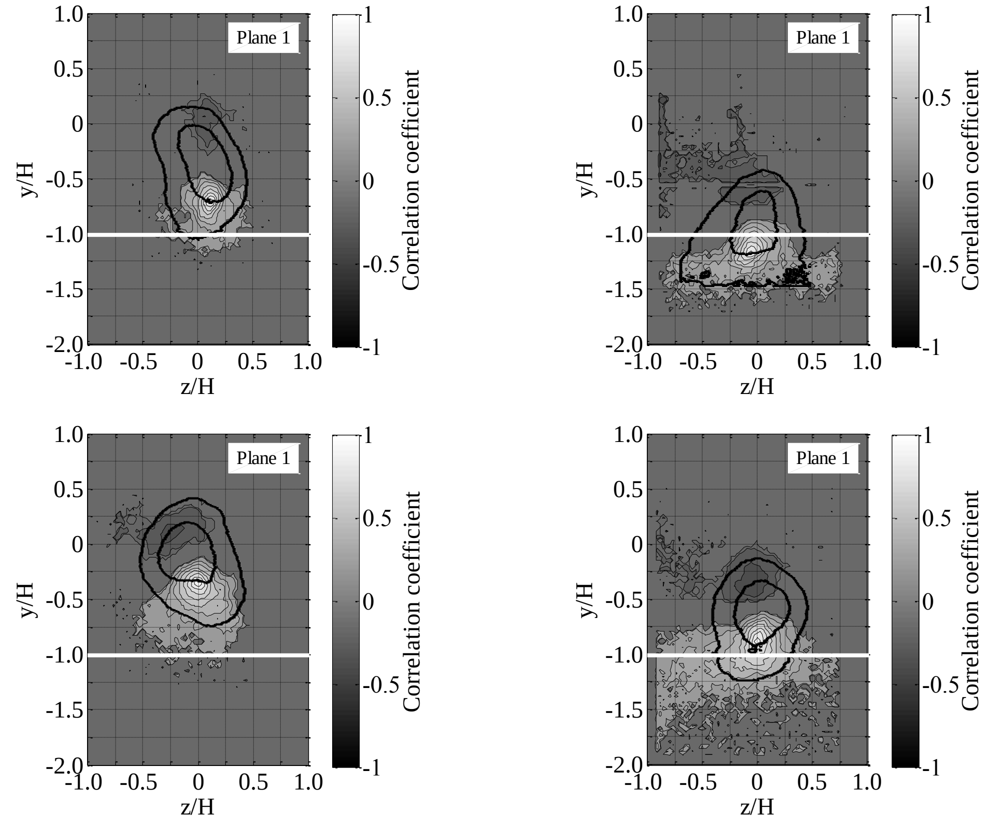

Fig. 15 Correlation maps in plane 1 for He-injection cases. (top left) P_{0j}=2.4 atm, with-pylon, (top right) P_{0j}=2.4 atm, without-pylon, (bottom left) P_{0j}=5.1 atm with-pylon, (bottom right) P_{0j}=5.1 atm, without-pylon.

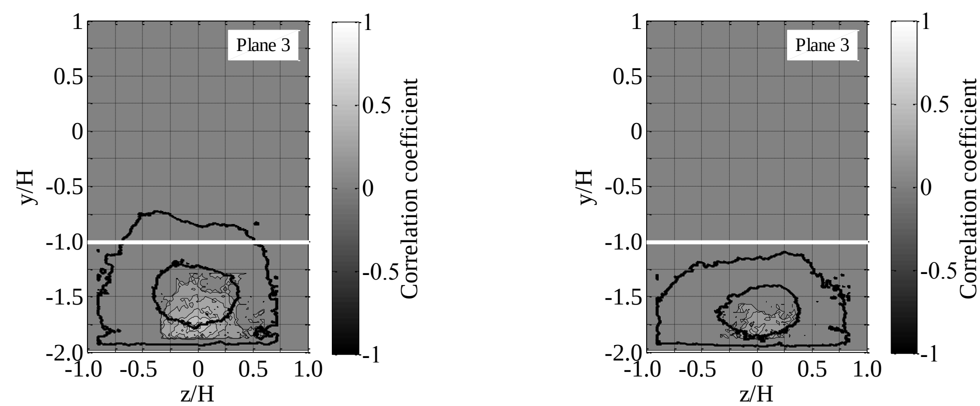

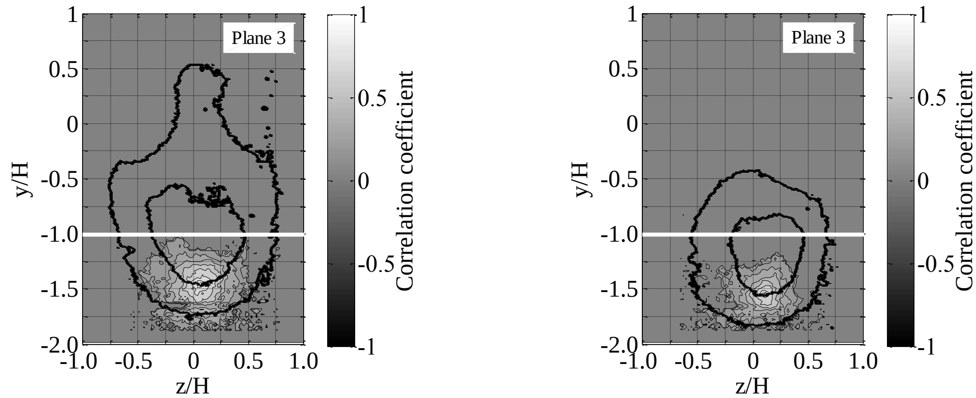

Fig. 16 Correlation maps in plane 3 for He-injection cases. (top left) P_{0j}=2.4 atm, with-pylon, (top right) P_{0j}=2.4 atm, without-pylon, (bottom left) P_{0j}=5.1 atm with-pylon, (bottom right) P_{0j}=5.1 atm, without-pylon.

Concluding Remarks

This study has shown that upstream pylon-aided injection into a Mach 1.6 air stream has been studied using PLIF with data recorded at three planes in a chamber behind a two-dimensional step. Injection pressures and injectants molecular weight were examined with emphasis on penetration, spreading and shape of the jet plume.

The study has shown that the difficult problem of predicting and tracking flameholding in high-speed flows must be followed both from the point of view of fueling schemes but also from the interaction between combustion chamber and the upstream isolator.

The results presented above have showen the following:

- The presence of thin pylon causes essentially no pressure loss.
- With the pylon all the jet is lifted from the injection wall with both penetration and spreading increasing. Penetration is increased more at higher injection pressure while spreading dominates at lower injection pressure.
- Without the pylon the injectant penetration relies only on the injection pressure but the injectants remain close to the wall with considerably increased spreading at the lower injection pressure.
- The injectant molecular weight has little effect on the jet penetration but the heavier injectant shows increased spreading when the pylon is absent.
- In the near-field the presence of the pylon leads to increased penetration and reduced spreading; however, in the far-field spreading is improved by other factors, notably by the large vortical structures induced by the presence of side walls.
- Statistical analysis conducted for He-injection indicated an enhanced dynamic behavior of the flow structure in the near-field, represented her by the plane closer to the step.
- The negative correlation region that appeared symmetrically relative to the plume center indicated that the fluid present in the upper part of the injectant cross-section is pushed into the step base region.
- With the pylon the highly correlated region is compact and well-organized, whereas without the pylon the region is not well organized and expands into the step base.
- In the far-field plane the highly correlated region is small for every case; this indicates that the large-scale turbulent structure is no longer prevalent in this plane due to improved mixing in the duct section upstream of the investigated plane.

References

[1] Segal, C., *The Scramjet Engine: Processes and Characteristics*, Cambridge University Press, Cambridge, United Kingdom, ISBN 0521838150, 2009.

[2] Seiner, J.M., Dash, S. M., and Kenzakovich, D.C., "Historical Survey on Enhanced Mixing in Scramjet Engines," *Journal of Propulsion and Power*, Vol. 17, No. 6, 2001, pp.1273-1286.

[3] Schetz, J. A., Maddalena, L., Throckmorton, R., and Neel, R., "Complex wall injector array for high-speed combustors," *Journal of Propulsion and Power*, Vol. 24, No. 4, 2008, pp.673-680.

[4] Northam, G. B., Greenberg, I., Byington, C. S, and Capriotti, D. P., "Evaluation of Parallel Injector Configurations for Mach 2 Combustion," *Journal of Propulsion and Power*, Vol. 8, No. 2, 1992, pp. 491-499.

[5] Hartfield, R. J., Hollo, S. D., and McDaniel, J. C., "Experimental Investigation of Swept Ramp Injector Using Laser-Induced Iodine Fluorescence," *Journal of Propulsion and Power*, Vol. 10, No. 1, 1994, pp. 129-135.

[6] Riggins, D.W., McClinton, C.R. Rogers, R. C., and Bittner, R. D., "Investigation of Scramjet Strategies for High Mach Number Flows," *Journal of Propulsion and Power*, Vol. 11, No. 3, 1995, pp. 409-418.

[7] Cox, S. K., Fuller, R. P., Schetz, J. A., and Walters, R. W., "Vortical Interaction Generated by an Injector Array to Enhance Mixing in Supersonic Flow," AIAA Paper 94-0708, Jan. 1994.

[8] Fuller, R. P., Wu, P. –K., Nejad, A. S., and Schetz, J. A., "Fuel-Voetrx Interaction for Enhanced Mixing in Supersonic Flow," AIAA Paper 96-2661, July 1996.

[9] Bowersox, R. D. W., "Turbulent Flow Structure Characterization of Angled Injection into a Supersonic Crossflow," *Journal of Propulsion and Power*, Vol. 34, No. 2, 1997, pp. 205-213.

[10] Thomas, R. H., Schetz, J. A., and Fuller, E.J., "Effects of Yaw on Low Angle Injection into a Supersonic Flow," AIAA Paper 1991-14, 1991.

[11] Vinogradov, V. A. and Prudnikov, A. G., "Injection of Liquid into the Strut Shadow at Supersonic Velocities," SAE Aerospace Altantic Conference, Society of Automotive Engineers, SAE-931455, 1993.

[12] Livingston, T., Segal, C., Schindler, M., and Vingogradov, V. A., "Penetration and Spreading of Liquid Jets in an External-Internal Compression Inlet," *Journal of Propulsion and Power*, Vol. 38, No. 6, 2000, pp.989-994.

[13] Schetz, J. A., "Turbulent Flowfield Mixing and Injection Process," in (Martin Summerfield, ed.), Vol. 68 of *Progress in Astronautics and Aeronautics*, AIAA.

[14] Vinogradov, V. A., Shikhman, Yu. M. and Segal, C., "A Review of Fuel Pre-injection in Supersonic, Chemically Reacting, Flows," *ASME Applied Mechanics Reviews*, Vol. 60, Issue 4, 2007, pp.139-148.

[15] Owens, M., Mullagiri, S., Segal, C., and Vinogradov, V. A., "Effects of Fuel Preinjection on Mixing in Mach 1.6 Airflow," *Journal of Propulsion and Power*, Vol. 17, No. 3, 2001, pp. 605-610.

[16] Shikhman, Yu. M., Vinogradov, V. A., Yanovskiy, L. S., Stepanov, V.A., Shlyakotin, V.E., and Penkov, S.N., "The Demonstration of Technologies-Endothermic Hydrocarbon Fueled dual Mode Scramjet," AIAA Paper 2001-1787, 2001.

[17] Vinogradov, V. A., Grachev, V., Petrov, M., and Sheechman, J. "Experimental Investigation of 2-D dual Mode Scramjet with Hydrogen Fuel at Mach 4-6," AIAA Paper 90-5269, 1990.

[18] Guoskov, O. V., Kopchenov, V. I., Lomkov, K. E., Vinogradov, V. A., and Waltrup, P. J., "Numerical Research of Gaseous Fuel Preinjection in Hypersonic Three Dimensional Inlet, " *Journal of Propulsion and Power*, Vol. 17, No. 6, 2001, pp.1162-1169.

[19] Gruber, M. R., Carter, C. D., Montes, D. R, Haubelt L. C., King, P. I., and Hsu, K.-Y., "Experimental Studies of Pylon-Aided Injection into a Supersonic Crossflow," *Journal of Propulsion and Power,* Vol. 24, No. 3, May-June 2008, pp. 460-470.

[20] Pohlman, M. R. and Greendyke, R. B., "Critical Design Parameters for Pylon-Aided Gaseous Fuel Injection" AIAA Paper 2009-1422, January 2009.

[21] Segal, C. and Young, C.D., "Development of an Experimentally Flexible Facility for Mixing-Combustion Interactions in Supersonic Flow", *ASME*, Vol. 118, June 1996, pp. 152-158.

[22] Takahashi, H., "Experimental Study of Scalar Structure in a Supersonic Turbulent Mixing Flowfield Using Acetone PLIF," Ph.D. Dissertation, Aerospace Engineering Dept., Tohoku Univ., Sendai, Japan, Mar. 2009.

[23] Thurber, M. C., "Acetone Laser-Induced Fluorescence for Temperature and Multiparameter Imaging in Gaseous Flows," Ph.D. Dissertation, Mechanical Engineering Dept., Stanford Univ., Stanford, CA, Mar. 1999.

[24] Tu, Q., and Segal, C., "Isolator/Combustion Chamber Interactions during Supersonic Combustion," AIAA Paper 2009-4845, August 2009.

[25] Thakur, A., and Segal, C., "Concentration Distribution in a Supersonic Flow Recirculation Region," *Journal of Propulsion and Power*, Vol. 24, No. 1, Jan. 2008, pp. 64-73.

[26] Ben-Yakar, A., Mungal, M. G., and Hanson, R. K., "Time Evolution and Mixing Characteristics of Hydrogen and Ethylene Transverse Jets in Supersonic Crossflows," *Physics of Fluids,* Vol. 18, 2006, pp. 026101.

[27] Smith, K. M., and Dutton, J.C., "Investigation of Large-Scale Structures in Supersonic Planar Base Flows," *AIAA Journal*, Vol. 34, No. 6, Jun. 1996, pp. 1146-1152.

[28] Schetz, J. A. and F.S. Billig, "Penetration of Gas Jets injected into a Supersonic Stream", *AIAA Journal*, Vol. 3, No. 11, Nov. 1966, pp. 1658-1665.
[29] Portz, R., and Segal, C., "Penetration of Gaseous Jets in Supersonic Flows," *AIAA Journal*, Vol. 44, No. 10, Oct. 2006, pp.2426-2429.
[30] Burger, S. K., Schetz, J. A., and Ungewitter, R., "Effects of Injectant Molecular Weight on Transverse Injection Mixing Processes in Supersonic Flow," AIAA Paper 2009-7315, 2009.
[31] Takahashi, H., Oso, H., Kouchi, T., Masuya, G., and Hirota, M., "Scalar Spatial Correlations in a Supersonic Mixing Flowfield," AIAA Paper 2009-0023, 2009.
[32] Messersmith, N. L., and Dutton, J. C., "Characteristic Features of Large Structures in Compressible Mixing Layers," *AIAA Journal*, Vol. 34, No. 9, Sep. 1996, pp. 1814-1821.